



CHORUS

This is the accepted manuscript made available via CHORUS. The article has been published as:

Using the carrier-envelope phase to control strong-field dissociation of $\text{HeH}^{\{+\}}$ at midinfrared wavelengths

D. Ursrey and B. D. Esry

Phys. Rev. A **96**, 063409 — Published 14 December 2017

DOI: [10.1103/PhysRevA.96.063409](https://doi.org/10.1103/PhysRevA.96.063409)

Using the carrier-envelope phase to control strong-field dissociation of HeH⁺ in the mid-infrared

D. Ursrey and B. D. Esry

J.R. Macdonald Laboratory, Kansas State University, Manhattan, Kansas 66506

(Dated: October 16, 2017)

We study the response of HeH⁺ to an intense, few-cycle laser pulse. Specifically, we present the carrier-envelope phase dependence of the kinetic energy release spectrum, the spatial asymmetry, and the total dissociation probability in two-cycle pulses with an intensity of 10¹⁴ W/cm² and wavelengths of 3200 nm and 4000 nm. Strong spatial asymmetries are found in spite of the fact that the electron always becomes localized as He+H⁺, demonstrating that control of such asymmetries can be obtained via control of the nuclear degrees of freedom — as opposed to its usual interpretation as control over the electronic degrees of freedom. We explain these CEP effects in terms of our photon-phase representation.

I. INTRODUCTION

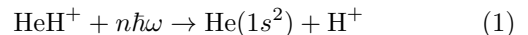
In the past few decades, there has been much focus on using intense, ultrafast laser pulses to control the dissociation of molecules. Theoretical studies of this nature have predicted that physical observables can be controlled by varying the delay between two pulses with different colors [1–4] or by varying the carrier-envelope phase (CEP) of a single-color pulse [5–9]. Specifically, studies focusing on the various isotopologues of H₂⁺ have shown that these forms of coherent control can be achieved for the kinetic energy release (KER) spectrum, momentum distribution, total dissociation probability, and spatial asymmetry of the dissociating fragments [3, 5, 6, 9–11]. Similar studies on CO have predicted that two-color pulses can be used to control molecular orientation [4, 12, 13]. These theoretical predictions have been realized in experiments starting from the neutral targets H₂ [14–18], D₂ [13, 15, 18–22], HD [19, 23], CO [4, 13, 24–26], DCl [27, 28], and small polyatomic molecules [29–37]. More recently, experimental CEP control has been demonstrated directly on H₂⁺ [38–40].

While theoretical and experimental results have conclusively shown that coherent control can be achieved using either the two-color phase or the CEP, there is still room for improvement in our understanding of the physical mechanisms responsible for this control, especially for the CEP. Considerable interpretive and predictive success has been achieved using our photon-phase representation [7, 9, 18, 39–43] to understand these two types of control in terms of interference between different photon pathways. This methodology has, for instance, been successfully applied to interpret results for CEP control of alkali atoms and xenon [42, 43] (respectively), for H₂ and D₂ [18, 41], and for H₂⁺ and its isotopologues [7, 9, 10, 39, 40]. Because the photon-phase representation depends only upon the incident field (and not the system itself), it can be employed to help us gain physical insight into CEP and two-color effects in *any* system, including more complicated atoms and molecules.

In this paper, we will take advantage of the generality of the photon-phase representation to extend our under-

standing of coherent control to a new system: HeH⁺, the simplest heteronuclear molecule with an electronic asymmetry in the standard Born-Oppenheimer approximation. We have previously shown [44] that exposing HeH⁺ to long-wavelength pulses (longer than roughly $\lambda = 2000$ nm) produces dissociation probabilities that are large enough to realistically measure provided the intensity approaches $I = 10^{14}$ W/cm². These relatively large dissociation probabilities, coupled with the fact that HeH⁺ ion beams have been shown to be viable experimental targets [45–47], make both experimental and theoretical studies on CEP control of HeH⁺ dissociation reasonable. Moreover, HeH⁺ is a particularly interesting molecule to study because its dissociation is dominated by permanent dipole effects in this regime [44]. This property makes HeH⁺ different from the vast majority of molecules studied in intense laser fields, which are dominated by electronic transitions.

In H₂⁺ and its isotopologues, CEP control of the spatial asymmetry of the H⁺+H dissociation fragments is often described as “controlling electron localization” [16–20]. In this paper, however, we demonstrate that a clear CEP-dependent spatial asymmetry can be observed in the strong-field process



even though the electron always localizes the same way—on the He atom—as it must since the dynamics occurs on a single electronic state. This system thus clearly illustrates the general principle that controlling the spatial asymmetry of dissociation fragments is actually controlling the nuclear degrees of freedom, not the electronic. This statement applies equally well to H₂⁺ once it is recognized that H₂⁺ can only dissociate into H⁺+H—*i.e.*, the electron always localizes to produce an H atom—and that the direction of the H⁺ is a continuous distribution. In other words, what is controlled is the direction of H⁺ just as for the present case of HeH⁺. Indeed, all control over the spatial asymmetry of dissociation is control over the nuclear degrees of freedom.

We will use numerical solutions of the time-dependent Schrödinger equation for HeH⁺ to show that CEP control can be exercised over the KER spectrum, the total

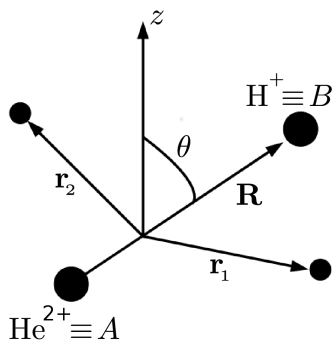


FIG. 1. Definition of the coordinates used in the Hamiltonian.

dissociation probability, and the spatial asymmetry of the dissociating fragments for pulses with intensities of 10^{14} W/cm² and wavelengths of 3200 and 4000 nm. The cause of, and relative magnitude of, the control of these observables is explained through our photon-phase representation.

II. THEORETICAL METHODS

A. Born-Oppenheimer representation for the time-dependent Schrödinger equation

We solve the time-dependent Schrödinger equation within the Born-Oppenheimer approximation. The methods used for the solution will be outlined here, but are described in more detail in our previous work [44, 48]. The electric field is treated classically, and the length gauge is used within the dipole approximation. Under these approximations, the time-dependent Schrödinger equation for HeH⁺ in an electric field \mathcal{E} is given by (atomic units will be used unless otherwise specified):

$$i \frac{\partial}{\partial t} \Psi(\mathbf{R}, \mathbf{r}_1, \mathbf{r}_2, t) = [T_N + H_{\text{el}} - \mathcal{E}(t) \cdot \mathbf{d}] \Psi(\mathbf{R}, \mathbf{r}_1, \mathbf{r}_2, t), \quad (2)$$

where T_N is the nuclear kinetic energy operator, \mathbf{d} is the dipole operator in the center-of-mass frame

$$\mathbf{d} = - \left(\frac{3 + m_A + m_B}{2 + m_A + m_B} \right) (\mathbf{r}_1 + \mathbf{r}_2) + \left(\frac{m_A - 2m_B}{m_A + m_B} \right) \mathbf{R}, \quad (3)$$

H_{el} is the electronic Hamiltonian (including the nuclear repulsion), and the coordinates are as shown in Fig. 1. For our calculations, we express the electric field as

$$\mathcal{E} = \mathcal{E}_0 e^{-(t/\tau)^2} \cos(\omega t + \varphi) \hat{\mathbf{z}}, \quad (4)$$

where φ is the CEP, ω is the carrier frequency, and $\tau = \tau_{\text{FWHM}}/\sqrt{2 \ln 2}$ with τ_{FWHM} being the full-width-at-half-maximum of the peak intensity. The electric field strength \mathcal{E}_0 is calculated from the peak intensity of the pulse as shown in the Ref. [49].

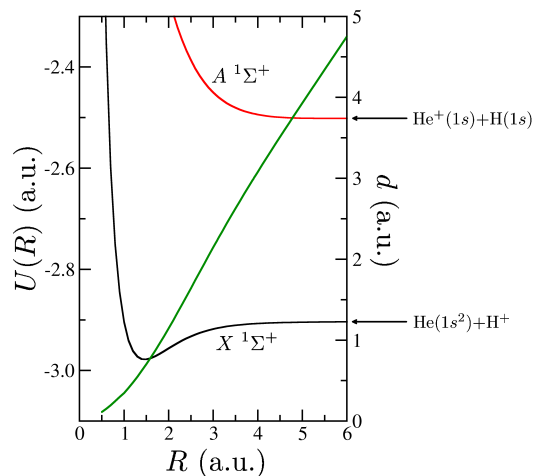


FIG. 2. The Born-Oppenheimer potential energy curves for the ground, $X^1\Sigma^+$, and first-excited, $A^1\Sigma^+$, singlet states of HeH⁺. The asymptotic products are indicated in each case. Also included is the $X^1\Sigma^+$ permanent dipole d (solid green line). All data is taken from Ref. [50].

We solve Eq. (2) within the Born-Oppenheimer approximation where the Born-Oppenheimer potentials and electronic wave functions are solutions of the eigenvalue problem

$$H_{\text{el}} \Phi_i(R; \mathbf{r}_1, \mathbf{r}_2) = U_i(R) \Phi_i(R; \mathbf{r}_1, \mathbf{r}_2). \quad (5)$$

For this work, we use the potentials and dipole matrix elements $d_{ij} = \langle \Phi_i | \mathbf{d} | \Phi_j \rangle$ from Ref. [50].

We simplify our calculations by taking advantage of the large difference in energy between the ground electronic potential $X^1\Sigma^+$ and the first-excited potential $A^1\Sigma^+$ as seen in Fig. 2. Because at least twenty-nine photons are required for electronic excitation at 3200 nm, and thirty-six at 4000 nm, we expect permanent dipole transitions to dominate over electronic excitation for the laser parameters considered. Consequently, we will neglect electronic excitation. Further justification of this one-channel approximation can be found in Ref. [44].

Writing the single electronic state as $\Phi \equiv \Phi_{X^1\Sigma^+}$, the total wave function can be written as

$$\Psi(\mathbf{R}, \mathbf{r}_1, \mathbf{r}_2, t) = \sum_J F_{JM}(R, t) Y_{JM}(\theta, \phi) \Phi(R; \mathbf{r}_1, \mathbf{r}_2). \quad (6)$$

In Eq. (6), θ and ϕ are the polar and azimuthal angles that describe the orientation of the molecular axis \mathbf{R} relative to the laboratory frame, M is the projection of the nuclear orbital angular momentum along the laser polarization, and J is the total orbital angular momentum. Our ability to write the wave function in this way depends on the facts that we have linearly polarized light, meaning only a single M is required, and that the sole electronic channel is a Σ state. For this work, we will consider only $M = 0$ initial states, allowing us to use the notation $F_{JM=0} \equiv F_J$ for the remainder of this paper.

Substituting Ψ into Eq. (2) and projecting out $Y_{J_0}\Phi$ gives the coupled differential equations that we must solve:

$$i\frac{\partial}{\partial t}F_J = \left[-\frac{1}{2\mu_{AB}}\frac{\partial^2}{\partial R^2} + \frac{J(J+1)}{2\mu_{AB}R^2} + U \right] F_J - \sum_{J'} \sqrt{\frac{4\pi}{3}} \mathcal{E}(t) d \langle Y_{J_0}|Y_{10}|Y_{J'_0} \rangle F_{J'}, \quad (7)$$

where the reduced mass is given by

$$\frac{1}{\mu_{AB}} = \frac{1}{m_A} + \frac{1}{m_B}. \quad (8)$$

In this work, we use ^4He and ^1H with masses $m_A=7351.67$ a.u. and $m_B=1836.15$ a.u., respectively. This isotope choice maximizes the magnitude of the permanent dipole [44]. Because it is truncated to only a single channel, there is no electronic coupling in Eq. (7) from either the external field or the field-free Coriolis coupling and non-Born-Oppenheimer effects.

B. Numerical details

To solve Eq. (7), we use the generalized finite differencing scheme from Ref. [51] (see also Ref. [52]) to find the ro-vibrational eigenstates of the field-free nuclear Hamiltonian. Individual ro-vibrational states are then propagated in the field using this generalized finite differencing along with split-operator techniques and the Crank-Nicolson method. This propagation scheme has been successfully used previously and is described in more detail in Refs. [48, 51, 53].

Our calculations are carried out for τ_{FWHM} equal to two cycles, using wavelengths of 3200 and 4000 nm with an intensity of 10^{14} W/cm². Calculations begin at the time t_i when the intensity of the field is 10^7 W/cm² and end at the time t_f , after the peak intensity, when the intensity falls to 10^8 W/cm². The time step is $\Delta t=0.008$ a.u., and we adaptively increase the number of partial waves used in the expansion of Ψ as explained in Ref. [48]. A non-uniform radial grid is used with $R_{\text{min}}=0.5$ a.u. and $R_{\text{max}}=110.0$ a.u. The grid points are initially defined with a grid spacing of $\Delta R \approx 0.002$ a.u. for $0.5 \text{ a.u.} \leq R \leq 10.0 \text{ a.u.}$ and $\Delta R \approx 0.009$ a.u. for $R > 10.0$ a.u. In order to smooth the abrupt change in grid spacing at $R=10.0$ a.u., we use the ad hoc procedure of three-point averaging. In this averaging, new grid points are defined by taking the average of each point with its two neighboring points (where all three points are weighted equally). One averaging pass through the grid is insufficient, so we make 20,000 such passes — determined from simple visual inspection and our own judgement. The exact number of passes is not critical because convergence testing in the number of grid points is carried out independent of the smoothing choice. All of our parameters were verified to produce three digits of convergence in the KER

spectrum up to an energy of 0.2 a.u. which is sufficient for all of the plots shown.

C. Momentum distribution in the photon-phase representation

Following our previous work [9], further insight into the CEP dependence of Ψ is gained by noting that the Hamiltonian—and, as a consequence, F_J —is periodic in φ . This allows us to write F_J *exactly* as a Fourier series, giving

$$F_J = \sum_n F_{nJ} e^{in\varphi}. \quad (9)$$

Here, F_{nJ} is independent of φ so that all CEP dependence is written explicitly. The summation index n in Eq. (9) can be interpreted as the net number of photons absorbed by the system [7, 9]. Because of this interpretation, we are able to infer which F_{nJ} must be exactly zero. For example, for an initial state with even J , we know from dipole selection rules that n and J must have the same parity—where parity here refers to whether the integers n and J are even or odd—for F_{nJ} to be nonzero. Similarly, for an initial state with odd J , we know that n and J must have different parity for F_{nJ} to be nonzero.

For this paper, we focus on CEP control of three physical observables: the spatial asymmetry of the dissociating fragments, the KER spectrum, and the total dissociation probability. All of these observables can be calculated from the distribution of the relative nuclear momentum \mathbf{k} , defined to point from the He atom to the proton, as seen in Fig. 1. In practice, we obtain these observables as described in Ref. [44]. The discussion here gives the framework for their interpretation.

After integrating over the momentum's azimuthal angle ϕ_k , the momentum distribution is

$$\begin{aligned} \frac{\partial^2 P}{\partial E \partial \theta_k} &= 2\pi \left| \langle \psi_{\mathbf{k}}^{(-)} | \Psi(t_f) \rangle \right|^2 \\ &= 2\pi \left| \sum_J (-i)^J e^{i\delta_J} Y_{J_0}(\theta_k) \langle EJ | F_J(t_f) \rangle \right|^2. \end{aligned} \quad (10)$$

Here, θ_k is the polar angle of \mathbf{k} measured relative to the laser polarization, $|\psi_{\mathbf{k}}^{(-)}\rangle$ is an energy-normalized field-free scattering state with asymptotic out-going momentum \mathbf{k} , and δ_J is the scattering phase shift for the energy-normalized field-free continuum state $|EJ\rangle$ with energy E and angular momentum J .

Using Eq. (9) for F_J in Eq. (10) and defining

$$A_{nJ}(E) = \sqrt{2\pi} (-i)^J e^{i\delta_J} \langle EJ | F_{nJ} \rangle, \quad (11)$$

we can write Eq. (10) within the photon-phase representation as:

$$\frac{\partial^2 P}{\partial E \partial \theta_k} = \sum_{n,J,J'} \left[A_{nJ} A_{nJ'}^* + \sum_{n' \neq n} A_{nJ} A_{n'J'}^* e^{i(n-n')\varphi} \right] Y_J Y_{J'}^*. \quad (12)$$

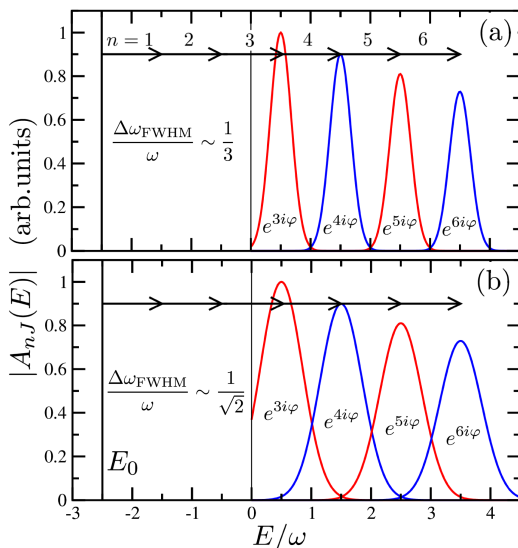


FIG. 3. Schematic illustration of the magnitudes $|A_{n,J}(E)|$, Eq. (11), in LOPT for the KER spectrum for photon processes with $n=3,4,5,6$ with the associated CEP-dependent phases indicated. (a) For a smaller relative bandwidth $\Delta\omega_{\text{FWHM}}/\omega$, there is some overlap between the peaks associated with n and $n\pm 1$ pathways, but the overlap between n and $n\pm 2$ pathways is very small. (b) The relative bandwidth is increased, which increases the overlap between n - and $(n\pm 1)$ -photon peaks as well as the n - and $(n\pm 2)$ -photon peaks. This larger overlap gives a larger product $A_{n,J}(E)A_{n',J'}(E)$ at the overlap energy, which increases the CEP control.

For brevity, we have used $Y_J \equiv Y_{J0}(\theta_k)$. We emphasize that all of the CEP dependence is explicit in the exponential factor. Moreover, the energy dependence is entirely contained within the amplitudes $A_{n,J}$; and the angular dependence, in Y_J . This expression and the others we derive apply generally to any single-channel system, including atomic ionization in the single-active-electron approximation.

Because n is the net number of photons [7, 9], $|A_{n,J}(E)|^2$ can be interpreted as the probability of exchanging n net photons with the field such that finally the energy is E and the angular momentum is J . We thus see from Eq. (12) that CEP effects can only be observed in the momentum distribution when there exists an energy E where the product $A_{n,J}A_{n',J'}^*$ is non-zero so that these two pathways can interfere. Dipole selection rules dictate that final states with $J-J'$ even must have $n-n'$ even, while final states with $J-J'$ odd must have $n-n'$ odd. Therefore, the former only produces CEP effects at an energy where pathways differing by at least two photons contribute, while the latter can create CEP effects at an energy where pathways differing by only one photon contribute.

A lowest-order-perturbation-theory (LOPT) picture gives a convenient way to visualize the physics involved at intensities where it at least roughly applies and is sketched in Fig. 3. The LOPT picture gives $|A_{n,J}(E)|^2$

peaked at $E \approx E_0 + n\omega$ with a profile determined generically by the power spectrum of the laser pulse. Where the different peaks overlap, CEP effects occur. A key parameter characterizing the potential magnitude of the CEP effects is thus the relative bandwidth $\Delta\omega_{\text{FWHM}}/\omega$. For the typical case of Gaussian peaks shown in Fig. 3, significant CEP effects generally require $\Delta\omega_{\text{FWHM}}/\omega$ larger than roughly $1/3$. At higher intensities, nonlinear shifts of the peak positions and profiles tend to increase the overlaps beyond the predictions of this simple picture. Nevertheless, the overlap between different photon pathways will generally be largest when $|\Delta n|$ is smallest.

We thus expect pathways with $|\Delta n|=1$ to have the largest overlap, giving a dominant CEP dependence of $\cos(\varphi + \varphi_1)$ where φ_1 is an energy-dependent offset phase that can be calculated from Eq. (12). These CEP effects will appear primarily at energies between the n -photon peaks as illustrated in Fig. 3 and will have $J-J'$ odd, yielding an angular distribution with a forward-backward asymmetry relative to the polarization direction. The overlap of $|\Delta n|=1$ peaks is thus the primary source of CEP-induced spatial asymmetry.

As the ratio $\Delta\omega_{\text{FWHM}}/\omega$ grows larger, the overlap between different photon peaks also increases, creating larger CEP effects. This increased overlap is illustrated in Fig 3(b). With a larger relative bandwidth, $|\Delta n|=2$ pathways begin to interfere. These effects will lie primarily at energies near the maximum of the intervening photon peak [see Fig. 3(b)]. And, since they have $J-J'$ even, the CEP dependence of their angular distribution is forward-backward symmetric. It follows that CEP control over yields is largely the result of $|\Delta n|=2$ pathway interference, therefore requiring much shorter pulses or higher intensities to be significant.

An important consequence of this picture is that for transform-limited pulses, $\Delta\omega_{\text{FWHM}}/\omega$ necessarily grows when the pulse is made shorter, thus increasing the overlap of n -photon peaks and the corresponding CEP effects. Similarly, if the pulse length is kept fixed, then $\Delta\omega_{\text{FWHM}}/\omega$ necessarily grows when the wavelength is increased, leading to larger CEP effects. In light of our photon-phase picture, though, we regard this enhancement as rather trivial. We have consequently fixed not the pulse length in our calculations, but rather the number of cycles in the pulse, thus assuring that $\Delta\omega_{\text{FWHM}}/\omega$ is fixed as we change the wavelength. Any wavelength influence over CEP effects that we find will therefore be due to the details of the system.

D. Kinetic energy release in the photon-phase representation

We may calculate the KER spectrum from the momentum distribution as

$$\begin{aligned} \frac{dP}{dE} &= \int_0^\pi \frac{\partial^2 P}{\partial E \partial \theta_k} \sin \theta_k d\theta_k \\ &= \frac{1}{2\pi} \sum_{n,J} \left[|A_{nJ}|^2 + \sum_{\substack{n' \neq n \\ n-n' \text{ even}}} A_{nJ} A_{n'J}^* e^{i(n-n')\varphi} \right]. \end{aligned} \quad (13)$$

Equation (13), unlike Eq. (12), allows only for interference of final states with the same angular momentum. Therefore, CEP effects can only occur in the KER spectrum when dissociation pathways $|\Delta n| \geq 2$ overlap in energy [9]. This means that the dominant CEP dependence in the KER spectrum is a linear combination of $\cos 2\varphi$ and $\sin 2\varphi$ and that the CEP effects found in the KER spectrum can generally be expected to be smaller than those found in the momentum distribution. Moreover, from Fig. 3, the CEP effects from $n+1$ interfering with $n-1$ will generally lie at energies near the n -photon peak, leading to small variations on a large signal.

To quantify the CEP effects in the energy spectrum, we use the normalized yield \mathcal{Y} ,

$$\mathcal{Y}(E) = \frac{dP}{dE} \left\langle \frac{dP}{dE} \right\rangle_\varphi^{-1}, \quad (14)$$

where $\langle dP/dE \rangle_\varphi$ is the CEP-averaged spectrum. Given our photon-phase analysis above, $\mathcal{Y}(E)$ can thus be parametrized as

$$\mathcal{Y} = 1 + \mathcal{Y}_2 \cos(2\varphi + \varphi_2) + \mathcal{Y}_4 \cos(4\varphi + \varphi_4) + \dots \quad (15)$$

Note that all of the \mathcal{Y}_n and φ_n are energy dependent and that the \mathcal{Y}_n give the relative magnitudes of the CEP effects.

E. Total dissociation probability in the photon-phase representation

We obtain the total dissociation probability by integrating the KER spectrum,

$$P = \int \frac{dP}{dE} dE. \quad (16)$$

Like the KER spectrum, the total dissociation probability only allows for interference of final states with the same angular momentum and $|\Delta n|$ even. Therefore, the total dissociation probability will have smaller CEP effects than the momentum distribution. Moreover, we expect that the CEP control over the total dissociation probability will also be smaller than that of the KER spectrum since the energy dependence of φ_n from Eq. (15) will lead to cancellations in the integral over energy. Indeed, our calculations show the CEP dependence of P in the cases studied for this paper to be quite small.

F. Spatial asymmetry in the photon-phase representation

The final observable that we study is the one most often used to characterize CEP effects, namely the normalized spatial asymmetry:

$$\mathcal{A}(E) = \left[P_{\text{up}}(E) - P_{\text{down}}(E) \right] \left\langle \frac{dP}{dE} \right\rangle_\varphi^{-1}, \quad (17)$$

where

$$P_{\text{up}} = \int_0^{\pi/2} \frac{\partial^2 P}{\partial E \partial \theta_k} \sin \theta_k d\theta_k \quad (18)$$

and

$$P_{\text{down}} = \int_{\pi/2}^\pi \frac{\partial^2 P}{\partial E \partial \theta_k} \sin \theta_k d\theta_k. \quad (19)$$

We note that in using the CEP-averaged KER in the denominator of Eq. (17) we have deviated from standard practice. The downside of this choice is that \mathcal{A} no longer strictly lies between -1 and 1 . However, we gain simplicity in interpretation since any CEP dependence in \mathcal{A} can now only come from the numerator (and we show below that dP/dE does have CEP dependence).

It can be shown that the numerator in Eq. (17) reduces to

$$P_{\text{up}} - P_{\text{down}} = \frac{1}{4\sqrt{\pi}} \sum_{\substack{n,J \text{ even} \\ n',J' \text{ odd}}} C_{JJ'} A_{nJ} A_{n'J'}^* e^{i(n-n')\varphi}. \quad (20)$$

The constant $C_{JJ'}$ resulting from the angular integration can be written in terms of Clebsch-Gordan coefficients as

$$C_{JJ'} = \sum_{L=|J-J'|}^{J+J'} \frac{\sqrt{(2J+1)(2J'+1)} \langle JJ'00|L0 \rangle}{\Gamma(\frac{2-L}{2}) \Gamma(\frac{3+L}{2})}. \quad (21)$$

The spatial asymmetry thus extracts the part of the momentum distribution that is lost in calculating the KER spectrum from Eq. (13)—namely, the piece with J and J' of opposite parity and antisymmetric with respect to $\theta_k = \pi/2$. In the KER spectrum, only the symmetric piece survives integration, but in $P_{\text{up}} - P_{\text{down}}$ the symmetric piece is eliminated by the subtraction in Eq. (17). This result holds true even if the integration in Eqs. (18) and (19) is carried out over only an angular cut, as opposed to the entire hemispheres, as long as the cuts are symmetric about $\pi/2$.

The fact that only terms with J and J' having different parity contribute to $P_{\text{up}} - P_{\text{down}}$ means that n and n' must also have different parity to contribute. As a result, \mathcal{A} has no CEP-independent terms and oscillates about $\mathcal{A} = 0$ with terms having periodicities 2π , $2\pi/3$, $2\pi/5$, and so on in the CEP. It is expected that the 2π periodicity will dominate for most systems because it results from interference between pathways with $|\Delta n| = 1$

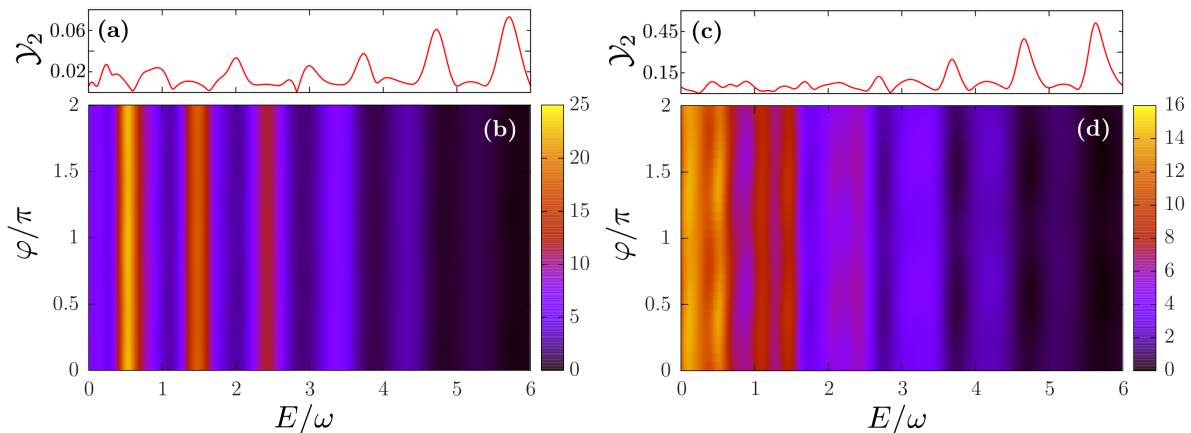


FIG. 4. (a) and (c): The relative amplitude \mathcal{Y}_2 of the CEP-dependent oscillation defined in Eq. (15) for (b) and (d), respectively. (b) and (d): KER spectrum dP/dE as a function of CEP in a 4000-nm pulse. Panels (a) and (b) are for $v=0$; and (c) and (d), for $v=1$.

which have a larger overlap than $|\Delta n| = 3$ pathways as illustrated in Fig. 3. Because photon pathways differing by only a single photon dominate \mathcal{A} , we expect to see larger CEP effects for \mathcal{A} than for the KER or total dissociation probability.

III. RESULTS AND DISCUSSION

Using the methods discussed in Secs. II A and II B, we calculated the components F_J of the final wave function. In principle, we could directly solve for the Fourier components F_{nJ} , but we chose to use the photon-phase representation only for our interpretation since a direct numerical solution in the photon-phase representation is much more demanding. Calculations are carried out for fixed initial vibrational states, all with $J = 0$. From F_J , the momentum distribution is calculated using Eq. (10) for a series of CEPs. All physical observables are calculated directly from the momentum distribution as described in Secs. II C–II F.

A. Kinetic energy release spectrum

The KER spectrum as a function of CEP is shown in Fig. 4(b) for a wavelength of 4000 nm and an initial state with $v = 0$. We clearly see the characteristic photon-spaced peaks of above-threshold dissociation (ATD) in the KER spectrum. Similar peaks were observed in our previous work [44]. This same behavior—ATD peaks with positions that are predicted by conservation of energy to a good approximation—is seen for all of the spectra that we calculated. From Fig. 4(b), we see that any CEP effects that occur in the KER spectrum are small.

We show \mathcal{Y}_2 from Eq. (15) in Figs. 4(a) and 4(c) for $v=0$ and $v=1$, respectively— \mathcal{Y}_4 and higher n are orders of

magnitude smaller in this energy range. In fact, even \mathcal{Y}_2 does not exceed a few percent except for regions where it is trivially enhanced by small signals. These small \mathcal{Y}_2 are due to the fact that the photon peaks differing by two or more photons are not broad enough to have significant overlap—and thus interference—for the laser parameters shown in the figure. This relative lack of CEP dependence is mirrored in all of our calculations for 3200 nm and most of our 4000-nm calculations.

Although \mathcal{Y}_2 remains less than 10% for $v=1$ at energies with substantial signal, it is larger than for $v=0$ —large enough that CEP effects can be seen in the CEP-dependent KER spectrum in Fig. 4(d). We believe that the appearance of visible CEP effects for this case is due to two different physical phenomena that increase the energy overlap of photon pathways: broadening of the KER peaks due to (i) multiphoton processes and (ii) resonance-enhanced multiphoton dissociation (REMPD).

1. Multiphoton peak broadening

The first phenomenon explains why CEP effects are more prominent for 4000 nm than 3200 nm in our calculations. Dissociation from $v = 0$ and $v = 1$ requires four and five photons for a 3200-nm pulse, respectively, while six and seven photons are required for a 4000-nm pulse. Since the width of the KER peaks generally increases with the order of the ATD peak, CEP effects at 4000 nm are favored over 3200 nm.

The dependence of the peak width on ATD peak order can be understood through the following simple picture (see Fig. 5). A given n -photon peak in the KER spectrum has a width due ultimately to the bandwidth of the laser pulse. Starting from any of the energies in this n -photon peak, an additional photon can be absorbed, giving rise to the $(n+1)$ -photon peak. This absorbed “photon” itself has a width due to the bandwidth of the laser pulse. The

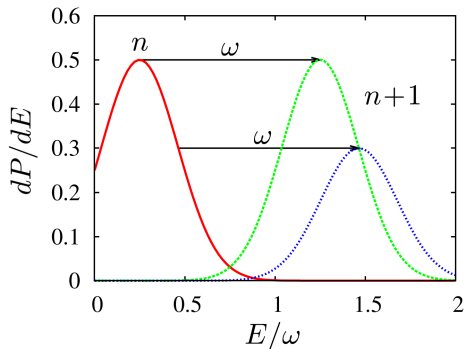


FIG. 5. Sketch of the KER spectrum, in arbitrary units, showing pathways producing the $(n+1)$ -photon peak based on the heuristic explanation in the text. The absorption of an additional photon beyond the n -photon peak originates from different energies within the peak, leading to a broadening of the $(n+1)$ -photon peak relative to the n -photon peak.

$(n+1)$ -photon peak finally observed in the KER spectrum is the sum of all transitions originating from every energy in the n -photon peak distribution—including, in reality, interference and resonance effects which are not accounted for in this simple picture. The resultant $(n+1)$ -photon peak is thus broader than the n -photon peak.

Quantifying this picture (as sketched in the Appendix), the $(n+1)$ -photon peak is a convolution of the n -photon peak with the laser's spectrum. Applying this result iteratively using the fact that the one-photon peak's width is $\Delta\omega$ to a good approximation, one can show that this picture predicts that the width of the n -photon peak for a Gaussian laser spectrum is proportional to $\sqrt{n}\Delta\omega$. Based on the empirical fact that in the closely-related phenomenon of above threshold ionization (ATI) photon peaks can be observed to very high orders, this simple picture likely overestimates the growth of the width.

This heuristic explanation suggests that for a given wavelength, CEP effects would be larger for $v = 0$ than for $v = 1$ because of the larger number of photons required for dissociation (one more photon for the wavelengths here). However, comparison of $v=0$ and $v=1$ in Fig. 4 shows that this is not always the case. This discrepancy suggests that there is a second physical mechanism responsible for CEP effects in the 4000-nm $v=1$ case, but not the $v=0$ case.

2. REMPDP peak broadening

As mentioned above, we believe that this second mechanism is REMPDP, a phenomenon we also identified in our previous calculations for HeH^+ at shorter wavelengths [44]. This conclusion is based on the telltale splitting of the individual KER peaks seen in Fig. 4(d) and its similarity to that seen in Ref. [44]. The additional peak is due to REMPDP, and we believe it proceeds in this case

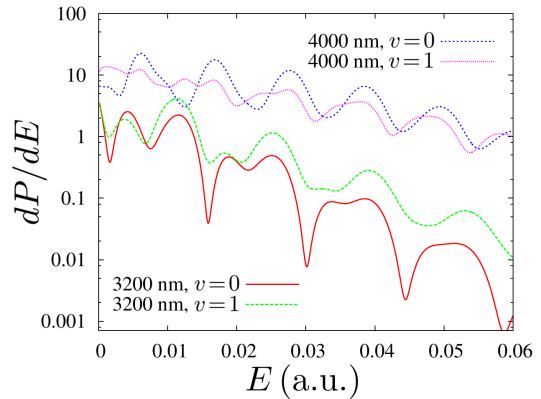


FIG. 6. KER spectra, dP/dE , in atomic units for $\varphi = \pi$ cuts of Figs. 4(b) and 4(d) along with the equivalent spectra for 3200 nm.

via the near-resonant transition between the initial state and the $v=2$, $J=1$ state ($E_{v=2, J=1} - E_{v=1, J=0} = 0.06\omega$). The splitting caused by REMPDP broadens the KER peaks as can be more clearly seen in Fig. 6, producing the larger CEP effects.

Resonant processes do cause structure in the individual KER peaks for other initial states and wavelengths as well, as shown in Fig. 6. However, this effect is largest for the 4000-nm, $v = 1$ case. Figure 6 shows that the peaks for this case are broad enough that there is much less-pronounced minimum between adjacent photon peaks and thus a larger overlap between the different photon pathways.

Recalling that CEP effects in the KER spectrum are due to the overlap of $|\Delta n| \geq 2$ pathways, we expect to see the largest—in an absolute sense—CEP effect at the energy of the KER peaks since the $(n-1)$ - and $(n+1)$ -photon peaks overlap exactly at the n -photon peak energy. This prediction is validated by Figs. 4(b) and 4(d), although Figs. 4(a) and 4(c) show that the relative CEP effect tends to be smaller at these energies. Moreover, because we expect interference between $|\Delta n|=2$ pathways to dominate, Eq. (13) tells us to expect π periodicity in the CEP dependence of our results. This also agrees with Fig. 4. We note that our predicted periodicity and energy of the CEP effect in the KER spectrum have been seen experimentally in H_2^+ [18, 39].

B. Total dissociation probability

The second observable of interest is the total dissociation probability. Our calculations confirm the π periodicity in P expected from Eqs. (13) and (16) that arises from the $|\Delta n|=2$ interference. We also find that the CEP effects are larger for 4000 nm than for 3200 nm which is convenient for potential experiments in the sense that the 4000-nm pulse produces the larger total dissociation probability. However, this also reduces the relative size of the effect, which is already small to begin with—in no

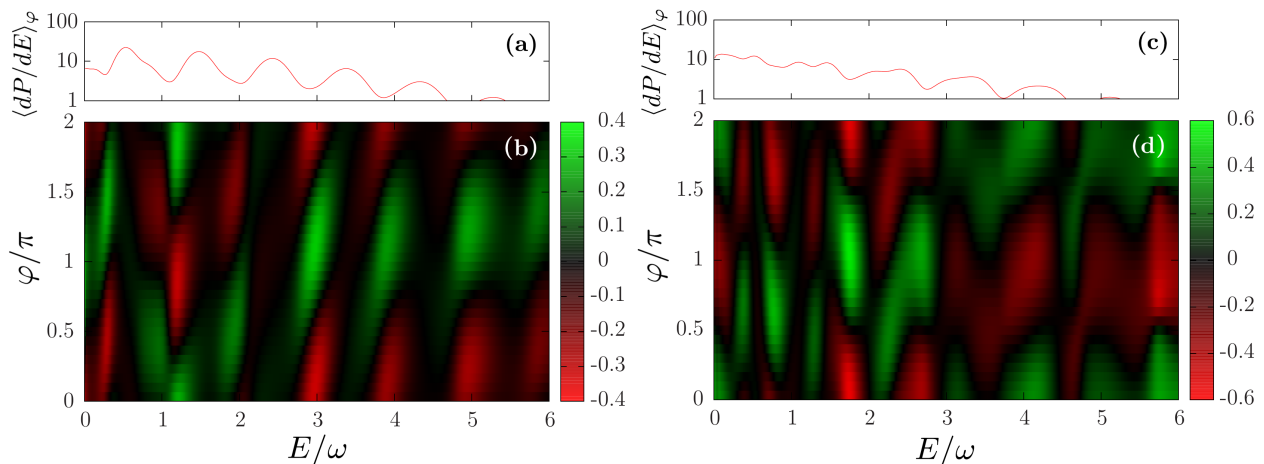


FIG. 7. (a) and (c): CEP-averaged KER spectrum, $\langle dP/dE \rangle_\varphi$, in atomic units for (b) and (d), respectively. (b) and (d): Normalized spatial asymmetry \mathcal{A} as a function of CEP and KER in a 4000-nm pulse. Panels (a) and (b) are for $v=0$; and (c) and (d), for $v=1$. Per the discussion in the text, the areas of largest spatial asymmetry generally occur between KER peaks, where the overlap between adjacent photon pathways is largest.

case did we find a modulation of P greater than 1% of $\langle P \rangle_\varphi$. The explanation for the 4000-nm pulse having the larger effect is the same as for the wavelength dependence of the KER spectrum.

C. Spatial asymmetry

Finally, we consider the spatial asymmetry, Eq. (17), which is shown in Fig. 7 for $v = 0$ and $v = 1$ in a 4000-nm pulse normalized by the CEP-averaged KER spectrum. Figure 7 shows energy-dependent peaks with 2π periodicity as predicted by Eq. (20) for the interference of pathways with $|\Delta n| = 1$. As expected for $|\Delta n|=1$ interference compared to $|\Delta n|=2$, the CEP dependence of the spatial asymmetry is much more apparent than that of the KER spectrum or the dissociation probability. Also as expected, the spatial asymmetry is larger for $v = 1$ than for $v = 0$ per the discussion of the KER spectra in Sec. III A.

The fact that the structure in \mathcal{A} shows energy dependence has been seen in previous calculations and in measurements for H_2 and H_2^+ [9, 16, 18, 20, 39, 40, 54]. Equation (20) shows that, in all cases, this energy dependence must be due to the phase of $A_{nJ}(E)$ and thus reflects details of the system's structure and dynamics.

The large spatial asymmetry that we see for HeH^+ is particularly interesting considering that CEP control over the spatial asymmetry of molecular dissociation is routinely equated with control over electron localization. Since the dynamics is governed by just the ground-state channel $X^1\Sigma^+$ that dissociates to $He(1s^2)+H^+$, however, the electrons *always* localize on the He atom during dissociation, independent of the CEP. Therefore, the CEP-dependent spatial asymmetry seen here has nothing to do with electron localization. Instead, the CEP-controlled

spatial asymmetry is actually control over the nuclear degrees of freedom.

IV. SUMMARY

In this work, we studied the use of mid-infrared two-cycle pulses for CEP control of HeH^+ . Because long-wavelength dissociation of HeH^+ is dominated by permanent dipole effects, this system is unique among the molecules typically used in strong-field coherent control studies. Therefore, it serves not only as a benchmark heteronuclear system, but also as a benchmark system for understanding the control of permanent dipole transitions in molecules. This single-channel system also demonstrates a CEP control over spatial asymmetry that is due to interference in the nuclear degrees of freedom and not control over the electronic localization.

We have demonstrated that the dissociation of HeH^+ can be controlled using the CEP of the incident laser pulse. Although the effects on the KER spectrum and total dissociation probability are small, the normalized spatial asymmetry for HeH^+ in a 4000-nm pulse is larger than that of D_2 and H_2 found in 5-fs and 4-fs (respectively), 800-nm and 720-nm (respectively) experiments at the same intensity [20, 34]. In our review of the literature, we were only able to find one study that produced a normalized spatial asymmetry comparable to those found in our study of HeH^+ : the 40% asymmetry found for the dissociative ionization of H_2 in 800-nm, 6-fs, CEP-stabilized pulses in the work of Xu *et al.* [18]. The size of the normalized spatial asymmetry and total dissociation probability for 4000-nm pulses, coupled with the viability of mid-infrared pulses [15, 22, 55–60] and the use of HeH^+ as an experimental target [45–47] allows for the possibility of experimental observation of these results.

ACKNOWLEDGMENTS

We are grateful for many useful discussions with the group of Dr. I. Ben-Itzhak on the experimental accessibility of HeH^+ , and for our discussions with Dr. G. Armstrong on the calculation of the momentum distribution and the application of the photon-phase representation in

HeH^+ . We are also grateful for the help of Dr. N. Vaeck and the authors of Ref. [50], who sent us their data for the dipole matrix elements of HeH^+ . The authors acknowledge support from the Chemical Sciences, Geosciences, and Biosciences Division, Office of Basic Energy Sciences, Office of Science, US Department of Energy.

-
- [1] M. Shapiro and P. Brumer, *Quantum Control of Molecular Processes, Second Edition* (Wiley-Interscience, 2012). URL <http://dx.doi.org/10.1002/9783527639700>
- [2] P. Brumer and M. Shapiro, "Laser control of molecular processes," *Annu. Rev. Phys. Chem.* **43**, 257 (1992). URL <http://arjournals.annualreviews.org/doi/abs/10.1146/annurev.pc.43.100192.001353>
- [3] E. Charron, A. Giusti-Suzor, and F. H. Mies, "Coherent control of isotope separation in HD^+ photodissociation by strong fields," *Phys. Rev. Lett.* **75**, 2815 (1995). URL <http://link.aps.org/doi/10.1103/PhysRevLett.75.2815>
- [4] S. De, I. Znakovskaya, D. Ray, F. Anis, N. G. Johnson, I. A. Bocharova, M. Magrakvelidze, B. D. Esry, C. L. Cocke, I. V. Litvinyuk, and M. F. Kling, "Field-free orientation of CO molecules by femtosecond two-color laser fields," *Phys. Rev. Lett.* **103**, 153002 (2009). URL <http://link.aps.org/doi/10.1103/PhysRevLett.103.153002>
- [5] F. Anis and B. D. Esry, "Enhancing the intense field control of molecular fragmentation," *Phys. Rev. Lett.* **109**, 133001 (2012). URL <https://link.aps.org/doi/10.1103/PhysRevLett.109.133001>
- [6] V. Roudnev, B. D. Esry, and I. Ben-Itzhak, "Controlling HD^+ and H_2^+ dissociation with the carrier-envelope phase difference of an intense ultrashort laser pulse," *Phys. Rev. Lett.* **93**, 163601 (2004). URL <http://link.aps.org/doi/10.1103/PhysRevLett.93.163601>
- [7] V. Roudnev and B. D. Esry, "General theory of carrier-envelope phase effects," *Phys. Rev. Lett.* **99**, 220406 (2007). URL <http://link.aps.org/doi/10.1103/PhysRevLett.99.220406>
- [8] X. M. Tong and C. D. Lin, "Dynamics of light-field control of molecular dissociation at the few-cycle limit," *Phys. Rev. Lett.* **98**, 123002 (2007). URL <http://link.aps.org/doi/10.1103/PhysRevLett.98.123002>
- [9] J. J. Hua and B. D. Esry, "The role of mass in the carrier-envelope phase effect for H_2^+ dissociation," *J. Phys. B* **42**, 085601 (2009). URL <http://stacks.iop.org/0953-4075/42/i=8/a=085601>
- [10] P. Lan, E. J. Takahashi, K. Liu, Y. Fu, and K. Midorikawa, "Carrier envelope phase dependence of electron localization in the multicycle regime," *New Journal of Physics* **15**, 063023 (2013). URL <http://stacks.iop.org/1367-2630/15/i=6/a=063023>
- [11] F. He, C. Ruiz, and A. Becker, "Control of electron excitation and localization in the dissociation of H_2^+ and its isotopes using two sequential ultrashort laser pulses," *Phys. Rev. Lett.* **99**, 083002 (2007). URL <http://link.aps.org/doi/10.1103/PhysRevLett.99.083002>
- [12] M. Spanner, S. Patchkovskii, E. Frumker, and P. Corkum, "Mechanisms of two-color laser-induced field-free molecular orientation," *Phys. Rev. Lett.* **109**, 113001 (2012). URL <http://link.aps.org/doi/10.1103/PhysRevLett.109.113001>
- [13] M. F. Kling, P. von den Hoff, I. Znakovskaya, and R. de Vivie-Riedle, "(sub-)femtosecond control of molecular reactions via tailoring the electric field of light," *Phys. Chem. Chem. Phys.* **15**, 9448 (2013). URL <http://dx.doi.org/10.1039/C3CP50591J>
- [14] X. Gong, P. He, Q. Song, Q. Ji, H. Pan, J. Ding, F. He, H. Zeng, and J. Wu, "Two-dimensional directional proton emission in dissociative ionization of h_2 ," *Phys. Rev. Lett.* **113**, 203001 (2014). URL <https://link.aps.org/doi/10.1103/PhysRevLett.113.203001>
- [15] V. Wanie, H. Ibrahim, S. Beaulieu, N. Thiré, B. E. Schmidt, Y. Deng, A. S. Alnaser, I. V. Litvinyuk, X.-M. Tong, and F. Légaré, "Coherent control of D_2/H_2 dissociative ionization by a mid-infrared two-color laser field," *J. Phys. B* **49**, 025601 (2016). URL <http://stacks.iop.org/0953-4075/49/i=2/a=025601>
- [16] M. Kremer, B. Fischer, B. Feuerstein, V. L. B. de Jesus, V. Sharma, C. Hofrichter, A. Rudenko, U. Thumm, C. D. Schröter, R. Moshhammer, and J. Ullrich, "Electron localization in molecular fragmentation of H_2 by carrier-envelope phase stabilized laser pulses," *Phys. Rev. Lett.* **103**, 213003 (2009). URL <http://link.aps.org/doi/10.1103/PhysRevLett.103.213003>
- [17] B. Fischer, M. Kremer, T. Pfeifer, B. Feuerstein, V. Sharma, U. Thumm, C. D. Schröter, R. Moshhammer, and J. Ullrich, "Steering the electron in H_2^+ by nuclear wave packet dynamics," *Phys. Rev. Lett.* **105**, 223001 (2010). URL <http://link.aps.org/doi/10.1103/PhysRevLett.105.223001>
- [18] H. Xu, J.-P. Maclean, D. E. Laban, W. C. Wallace, D. Kielpinski, R. T. Sang, and I. V. Litvinyuk, "Carrier-envelope-phase-dependent dissociation of hydrogen," *New Journal of Physics* **15**, 023034 (2013). URL <http://stacks.iop.org/1367-2630/15/i=2/a=023034>

- [19] M. F. Kling, Siedschlag, Ch., I. Znakovskaya, A. J. Verhoef, S. Zherebtsov, F. Krausz, M. Lezius, and M. J. J. Vrakking, “Strong-field control of electron localisation during molecular dissociation,” *Mol. Phys.* **106**, 455 (2008).
URL <http://www.tandfonline.com/doi/abs/10.1080/00268970701864739>
- [20] M. F. Kling, Ch. Siedschlag, A. J. Verhoef, J. I. Kahn, M. Schultze, Y. Ni, Th. Uphues, M. Uiberacker, M. Drescher, F. Krausz, and M. J. J. Vrakking, “Control of electron localization in molecular dissociation,” *Science* **312**, 246 (2006).
URL <http://www.sciencemag.org/content/312/5771/246.abstract>
- [21] D. Ray, F. He, S. De, W. Cao, H. Mashiko, P. Ranitovic, K. P. Singh, I. Znakovskaya, U. Thumm, G. G. Paulus, M. F. Kling, I. V. Litvinyuk, and C. L. Cocke, “Ion-energy dependence of asymmetric dissociation of D_2 by a two-color laser field,” *Phys. Rev. Lett.* **103**, 223201 (2009).
URL <http://link.aps.org/doi/10.1103/PhysRevLett.103.223201>
- [22] I. Znakovskaya, P. von den Hoff, G. Marcus, S. Zherebtsov, B. Bergues, X. Gu, Y. Deng, M. J. J. Vrakking, R. Kienberger, F. Krausz, R. de Vivie-Riedle, and M. F. Kling, “Subcycle controlled charge-directed reactivity with few-cycle midinfrared pulses,” *Phys. Rev. Lett.* **108**, 063002 (2012).
URL <https://link.aps.org/doi/10.1103/PhysRevLett.108.063002>
- [23] B. Sheehy, B. Walker, and L. F. DiMauro, “Phase control in the two-color photodissociation of HD^+ ,” *Phys. Rev. Lett.* **74**, 4799 (1995).
URL <http://link.aps.org/doi/10.1103/PhysRevLett.74.4799>
- [24] K. J. Betsch, N. G. Johnson, B. Bergues, M. Kübel, O. Herrwerth, A. Senfleben, I. Ben-Itzhak, G. G. Paulus, R. Moshhammer, J. Ullrich, M. F. Kling, and R. R. Jones, “Controlled directional ion emission from several fragmentation channels of co driven by a few-cycle laser field,” *Phys. Rev. A* **86**, 063403 (2012).
URL <http://link.aps.org/doi/10.1103/PhysRevA.86.063403>
- [25] Y. Liu, X. Liu, Y. Deng, C. Wu, H. Jiang, and Q. Gong, “Selective steering of molecular multiple dissociative channels with strong few-cycle laser pulses,” *Phys. Rev. Lett.* **106**, 073004 (2011).
URL <http://link.aps.org/doi/10.1103/PhysRevLett.106.073004>
- [26] I. Znakovskaya, P. von den Hoff, S. Zherebtsov, A. Wirth, O. Herrwerth, M. J. J. Vrakking, R. de Vivie-Riedle, and M. F. Kling, “Attosecond control of electron dynamics in carbon monoxide,” *Phys. Rev. Lett.* **103**, 103002 (2009).
URL <http://link.aps.org/abstract/PRL/v103/e103002>
- [27] I. Znakovskaya, P. von den Hoff, N. Schirmel, G. Urbasch, S. Zherebtsov, B. Bergues, R. de Vivie-Riedle, K.-M. Weitzel, and M. F. Kling, “Waveform control of orientation-dependent ionization of dcl in few-cycle laser fields,” *Phys. Chem. Chem. Phys.* **13**, 8653 (2011).
URL <http://dx.doi.org/10.1039/C0CP02743J>
- [28] H. Li, X. M. Tong, N. Schirmel, G. Urbasch, K. J. Betsch, S. Zherebtsov, F. Smann, A. Kessel, S. A. Trushin, G. G. Paulus, K.-M. Weitzel, and M. F. Kling, “Intensity dependence of the dissociative ionization of dcl in few-cycle laser fields,” *J. Phys. B* **49**, 015601 (2016).
URL <http://stacks.iop.org/0953-4075/49/i=1/a=015601>
- [29] D. Mathur, K. Dota, A. K. Dharmadhikari, and J. A. Dharmadhikari, “Carrier-envelope-phase effects in ultrafast strong-field ionization dynamics of multielectron systems: Xe and CS_2 ,” *Phys. Rev. Lett.* **110**, 083602 (2013).
URL <http://link.aps.org/doi/10.1103/PhysRevLett.110.083602>
- [30] X. Xie, K. Doblhoff-Dier, S. Roither, M. S. Schöffler, D. Kartashov, H. Xu, T. Rathje, G. G. Paulus, A. Baltuška, S. Gräfe, and M. Kitzler, “Attosecond-recollision-controlled selective fragmentation of polyatomic molecules,” *Phys. Rev. Lett.* **109**, 243001 (2012).
URL <https://link.aps.org/doi/10.1103/PhysRevLett.109.243001>
- [31] A. Alnaser, M. Kübel, R. Siemering, B. Bergues, N. G. Kling, K. Betsch, Y. Deng, J. Schmidt, Z. Alahmed, A. Azzeer, J. Ullrich, I. Ben-Itzhak, R. Moshhammer, U. Kleineberg, F. Krausz, R. de Vivie-Riedle, and M. F. Kling, “Subfemtosecond steering of hydrocarbon deprotonation through superposition of vibrational modes,” *Nat. Commun.* **5**, 3800 (2014).
URL <http://dx.doi.org/10.1038/ncomms4800>
- [32] M. Kübel, A. S. Alnaser, B. Bergues, T. Pischke, J. Schmidt, Y. Deng, C. Jendrzewski, J. Ullrich, G. G. Paulus, A. M. Azzeer, U. Kleineberg, R. Moshhammer, and M. F. Kling, “Strong-field control of the dissociative ionization of N_2O with near-single-cycle pulses,” *New Journal of Physics* **16**, 065017 (2014).
URL <http://stacks.iop.org/1367-2630/16/i=6/a=065017>
- [33] M. Kübel, R. Siemering, C. Burger, N. G. Kling, H. Li, A. S. Alnaser, B. Bergues, S. Zherebtsov, A. M. Azzeer, I. Ben-Itzhak, R. Moshhammer, R. de Vivie-Riedle, and M. F. Kling, “Steering proton migration in hydrocarbons using intense few-cycle laser fields,” *Phys. Rev. Lett.* **116**, 193001 (2016).
URL <https://link.aps.org/doi/10.1103/PhysRevLett.116.193001>
- [34] H. Li, N. G. Kling, B. Förg, J. Stierle, A. Kessel, S. A. Trushin, M. F. Kling, and S. Kaziannis, “Carrier-envelope phase dependence of the directional fragmentation and hydrogen migration in toluene in few-cycle laser fields,” *Structural Dynamics* **3**, 043206 (2016).
URL <http://dx.doi.org/10.1063/1.4941601>
- [35] E. Lötstedt and K. Midorikawa, “Laser-induced electron localization in a triatomic molecular ion,” *Phys. Rev. A* **88**, 041402 (2013).
URL <https://link.aps.org/doi/10.1103/PhysRevA.88.041402>
- [36] E. Lötstedt and K. Midorikawa, “Carrier-envelope phase control of electron motion in laser-driven H_3^{2+} ,” *J. Phys. B* **47**, 204018 (2014).
URL <http://stacks.iop.org/0953-4075/47/i=20/a=204018>
- [37] M. Kübel, C. Burger, R. Siemering, N. G. Kling, B. Bergues, A. S. Alnaser, I. Ben-Itzhak, R. Moshhammer, R. de Vivie-Riedle, and M. F. Kling, “Phase- and intensity-dependence of ultrafast dynamics in hydro-

- carbon molecules in few-cycle laser fields,” *Molecular Physics* **115**, 1835 (2017).
URL <http://dx.doi.org/10.1080/00268976.2017.1288935>
- [38] H. Xu, H. Hu, X.-M. Tong, P. Liu, R. Li, R. T. Sang, and I. V. Litvinyuk, “Coherent control of the dissociation probability of h_2^+ in ω - 3ω two-color fields,” *Phys. Rev. A* **93**, 063416 (2016).
URL <https://link.aps.org/doi/10.1103/PhysRevA.93.063416>
- [39] T. Rathje, A. M. Sayler, S. Zeng, P. Wustelt, H. Figger, B. D. Esry, and G. G. Paulus, “Coherent control at its most fundamental: Carrier-envelope-phase-dependent electron localization in photodissociation of a h_2^+ molecular ion beam target,” *Phys. Rev. Lett.* **111**, 093002 (2013).
URL <https://link.aps.org/doi/10.1103/PhysRevLett.111.093002>
- [40] N. G. Kling, K. J. Betsch, M. Zohrabi, S. Zeng, F. Anis, U. Ablikim, B. Jochim, Z. Wang, M. Kübel, M. F. Kling, K. D. Carnes, B. D. Esry, and I. Ben-Itzhak, “Carrier-envelope phase control over pathway interference in strong-field dissociation of h_2^+ ,” *Phys. Rev. Lett.* **111**, 163004 (2013).
URL <https://link.aps.org/doi/10.1103/PhysRevLett.111.163004>
- [41] H. Xu, T.-Y. Xu, F. He, D. Kielpinski, R. T. Sang, and I. V. Litvinyuk, “Effect of nuclear mass on carrier-envelope-phase-controlled electron localization in dissociating molecules,” *Phys. Rev. A* **89**, 041403 (2014).
URL <https://link.aps.org/doi/10.1103/PhysRevA.89.041403>
- [42] F. Anis and B. D. Esry, “Enhancement of carrier-envelope phase effects in photoexcitation of alkali atoms,” *J. Phys. B* **42**, 191001 (2009).
URL <http://stacks.iop.org/0953-4075/42/i=19/a=191001>
- [43] K. S. Kang, K. Kim, J. hwan Lee, J. Lee, C. M. Kim, and C. H. Nam, “Carrier-envelope-phase-dependent above-threshold ionization of xenon observed with multi-cycle laser pulses,” *Opt. Express* **22**, 3684 (2014).
URL <http://www.opticsexpress.org/abstract.cfm?URI=oe-22-3-3684>
- [44] D. Ursrey, F. Anis, and B. D. Esry, “Multiphoton dissociation of HeH^+ below the $\text{He}^+(1s)+\text{H}(1s)$ threshold,” *Phys. Rev. A* **85**, 023429 (2012).
URL <http://dx.doi.org/10.1103/PhysRevA.85.023429>
- [45] I. Ben-Itzhak, I. Gertner, O. Heber, and B. Rosner, “Experimental evidence for the existence of the $2p\sigma$ bound state of heh^{2+} and its decay mechanism,” *Phys. Rev. Lett.* **71**, 1347 (1993).
URL <https://link.aps.org/doi/10.1103/PhysRevLett.71.1347>
- [46] I. Ben-Itzhak, Z. Chen, B. D. Esry, I. Gertner, O. Heber, C. D. Lin, and B. Rosner, “Mean lifetime of the bound $2p\sigma$ state of HeH^{2+} ,” *Phys. Rev. A* **49**, 1774 (1994).
URL <http://link.aps.org/doi/10.1103/PhysRevA.49.1774>
- [47] H. B. Pedersen, S. Altevogt, B. Jordon-Thaden, O. Heber, M. L. Rappaport, D. Schwalm, J. Ullrich, D. Zajfman, R. Treusch, N. Guerassimova, M. Martins, J.-T. Hoefl, M. Wellhöfer, and A. Wolf, “Crossed beam photodissociation imaging of HeH^+ with vacuum ultraviolet free-electron laser pulses,” *Phys. Rev. Lett* **98**, 223202 (2007).
URL <http://link.aps.org/doi/10.1103/PhysRevLett.98.223202>
- [48] F. Anis and B. D. Esry, “Role of nuclear rotation in dissociation of H_2^+ in a short laser pulse,” *Phys. Rev. A* **77**, 033416 (2008).
URL <http://link.aps.org/doi/10.1103/PhysRevA.77.033416>
- [49] The field strength in atomic units is defined as $\mathcal{E}=\sqrt{I/3.5\times 10^{16}\text{ W/cm}^2}$ with I the laser intensity.
- [50] J. Loreau, J. Liévin, P. Palmeri, P. Quinet, and N. Vaeck, “*Ab initio* calculation of the 66 low-lying electronic states of HeH^+ : adiabatic and diabatic representations,” *J. Phys. B* **43**, 065101 (2010).
URL <http://stacks.iop.org/0953-4075/43/i=6/a=065101>
- [51] M. W. J. Bromley and B. D. Esry, “Classical aspects of ultracold atom wave packet motion through microstructured waveguide bends,” *Phys. Rev. A* **69**, 053620 (2004).
URL <http://link.aps.org/doi/10.1103/PhysRevA.69.053620>
- [52] S. E. Koonin, K. T. R. Davies, V. Maruhn-Rezwani, H. Feldmeier, S. J. Krieger, and J. W. Negele, “Time-dependent hartree-fock calculations for $^{16}\text{O}+^{16}\text{O}$ and $^{40}\text{Ca}+^{40}\text{Ca}$ reactions,” *Phys. Rev. C* **15**, 1359 (1977).
URL <http://link.aps.org/doi/10.1103/PhysRevC.15.1359>
- [53] P. Q. Wang, A. M. Sayler, K. D. Carnes, J. F. Xia, M. A. Smith, B. D. Esry, and I. Ben-Itzhak, “Dissociation of H_2^+ in intense femtosecond laser field studied by coincidence 3D momentum imaging,” *Phys. Rev. A* **74**, 043411 (2006).
URL <http://link.aps.org/doi/10.1103/PhysRevA.74.043411>
- [54] V. Roudnev and B. D. Esry, “ hd^+ in a short strong laser pulse: Practical consideration of the observability of carrier-envelope phase effects,” *Phys. Rev. A* **76**, 023403 (2007).
URL <http://link.aps.org/doi/10.1103/PhysRevA.76.023403>
- [55] P. Colosimo, G. Doumy, C. I. Blaga, J. Wheeler, C. Hauri, F. Catoire, J. Tate, R. Chirla, A. M. March, G. G. Paulus, H. G. Muller, P. Agostini, and L. F. DiMauro, “Scaling strong-field interactions towards the classical limit,” *Nature Physics* **4**, 386 (2008).
URL <http://dx.doi.org/10.1038/nphys914>
- [56] C. I. Blaga, F. Catoire, P. Colosimo, G. G. Paulus, H. G. Muller, P. Agostini, and L. F. DiMauro, “Strong-field photoionization revisited,” *Nature Physics* **5**, 335 (2009).
URL <http://dx.doi.org/10.1038/nphys1228>
- [57] B. Bergues, S. Zherebtsov, Y. Deng, X. Gu, I. Znakovskaya, R. Kienberger, F. Krausz, G. Marcus, and M. F. Kling, “Sub-cycle electron control in the photoionization of xenon using a few-cycle laser pulse in the mid-infrared,” *New Journal of Physics* **13**, 063010 (2011).
URL <http://stacks.iop.org/1367-2630/13/i=6/a=063010>
- [58] Petersen Christian Rosenberg, Mller Uffe, Kubat Irnis, Zhou Binbin, Dupont Sune, Ramsay Jacob, Benson Trevor, Sujecki Slawomir, Abdel-Moneim Nabil, Tang

Zhuoqi, Furniss David, Seddon Angela, and Bang Ole, “Mid-infrared supercontinuum covering the 1.413.3 m molecular fingerprint region using ultra-high na chalco-genide step-index fibre,” *Nature Photonics* **8**, 830834 (2014).

URL <http://www.nature.com/nphoton/journal/v8/n11/abs/nphoton.2014.213.html#supplementary-information>

- [59] F. Silva, D. Austin, A. Thai, M. Baudisch, M. Hemmer, D. Faccio, A. Couairon, and J. Biegert, “Multi-octave supercontinuum generation from mid-infrared filamentation in a bulk crystal,” *Nat. Commun.* **3**, 807 (2012).

URL <http://dx.doi.org/10.1038/ncomms1816>

- [60] A. Thai, M. Hemmer, P. K. Bates, O. Chalus, and J. Biegert, “Sub-250-mrad, passively carrier-envelope-phase-stable mid-infrared opcpa source at high repetition rate,” *Opt. Lett.* **36**, 3918 (2011).

URL <http://ol.osa.org/abstract.cfm?URI=ol-36-19-3918>

Appendix A: Convolution approximation

To see that the energy dependence of the $(n+1)$ -photon peak can be obtained as a convolution of the n -photon peak with the laser pulse’s spectrum, we convert the sketch in Fig. 5 into mathematics. We denote the n -photon peak probability distribution by $P_n(E)$ and the

laser’s power spectrum as $P(E)$. The former peaks at E_n ; and the latter, at ω .

The distribution for both of the new peaks (green dashed and blue dotted lines) depicted in Fig. 5 is just the laser’s power spectrum, but based on different starting energies E'_i within $P_n(E)$ (red solid line) and weighted by the probability for this energy, $P_n(E'_i)$. Thus, the distribution for each of these new peaks is $P_n(E'_i)P(E - E'_i)$. Consequently, $P_{n+1}(E)$ is approximately

$$P_{n+1}(E) \approx P_n(E'_1)P(E - E'_1) + P_n(E'_2)P(E - E'_2) \quad (\text{A1})$$

when just the two peaks in Fig. 5 are taken into account. Since all values of E' within $P_n(E)$ should be used, we take the continuum limit to obtain

$$P_{n+1}(E) = \int dE' P_n(E')P(E - E'). \quad (\text{A2})$$

Thus, in this simple picture, the $(n+1)$ -photon peak distribution is a convolution of the n -photon peak with the laser’s power spectrum.

This picture is intended as a heuristic explanation of the broadening of the photon peaks with increasing order. It neglects, however, physics important for actually calculating the spectrum, including time-ordering, interference, resonances, and any energy dependence of the various dipole matrix elements needed.